

Stability Assessment of a Bedding Rock Slope Using Q-slope and Seismic Tomography: A Case Study in the Ecuadorian Amazon

Jorge Espin^{1*}, Sebastián Araujo¹

¹ Geophysics and Geotechnics Research Group, Earth and Water Sciences Faculty, Ikiam Universidad Regional Amazónica, 7 km from Muyuna, Napo, Ecuador

* Corresponding author, e-mail: jorge.espin@ikiam.edu.ec

Received: 26 July 2021, Accepted: 23 October 2021, Published online: 05 November 2021

Abstract

Roads are generally affected by slope failures, and these failures can increase when there are weathered materials and high rainfall. These circumstances occur in the sub-Andean zone of Ecuador. This is the region where the study area is located. The stability of a stratified rock slope, which is affecting a section of highway E45, was evaluated. The study slope is exposed to the road, but the upper part is covered by a soil-type material and dense vegetation that makes it challenging to study. We applied the Q-slope method and seismic tomography; these methods used together worked well, because they allowed to correlate and infer information about the quality of the rock mass, even in a fast and economical way. We also performed core drilling with core recovery in the crown of the slope and SPT test. The slope presented two well-differentiated zones; therefore, Q-slope values were calculated for each of these zones. The results show that the slope is unstable. The application of seismic tomography as an input parameter for calculating Q-slope was important because it allowed evaluating the stability where it is impossible to collect geomechanical information, correlate information taken at the foot of the slope, and define the depth of the bedrock.

Keywords

Q-slope, rock slope, seismic tomography, Napo Formation, Amazon Highway

1 Introduction

In this work, we use seismic tomography images to obtain the quality parameter of the mass rock. Many seismic surveys worldwide show the uses of this technique to know the rock quality in diverse geological formations. For example, the seismic refraction profiles are used in Singapore granite bedrock [1] and in the limestones, gypsiferous shale, and red marl in the Bidu Formation of Iran [2]. The seismic refraction tomography is used in soft sedimentary carbonatic rocks of the karst in south-eastern Italy [3] and the outcrops of sandstone and shale in Malaysian high-ways [4]. The borehole seismic tomography is also helpful for testing bridge foundations over Himalayan terrain with dolomite and limestone rocks [5]. In the specific case of using seismic tomography in the rock slopes quality determination, we have a 2D and 3D survey in an unstable mountain slope with three kinds of gneiss in the Swiss Alps [6]. Also, acoustic testing in the dam slopes of basalt and marble in China gives a reasonable determination of the P wave velocity to explore the rock mass properties [7]. Finally, a survey in Northeast

Turkey with the same seismic equipment used in our study, the Geometrics ES-3000, obtains seismic refraction tomography images in a slope formed by pyroclastic and dacitic volcano rocks [8].

The slope described in our study is located in the province of Napo, regionally located in the north of the sub-Andean zone of Ecuador, at the foothills of the Eastern Cordillera, formed by tectonically uplifted terrain and characterized by very intense seismic and volcanic activity, as well as erosion processes in the form of landslides (Fig. 1) [9].

The lithology of the slope corresponds to the Napo formation of the Cretaceous age, composed of a sequence of grey to black shales with intercalations of limestones and sandstones, possibly the most important formation in eastern Ecuador due to its oil interest [10]. This formation crosses Ecuador with an N-S orientation. Therefore, it is exposed in several sections of the E45 road and some secondary roads in the eastern provinces by reviewing the geologic map of Ecuador [11].

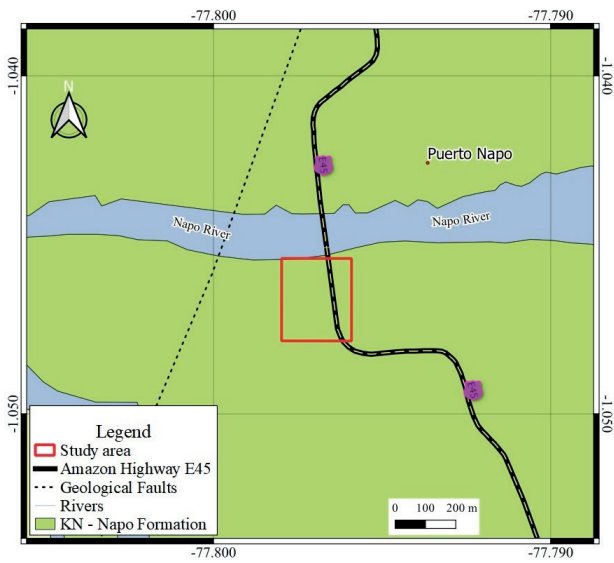
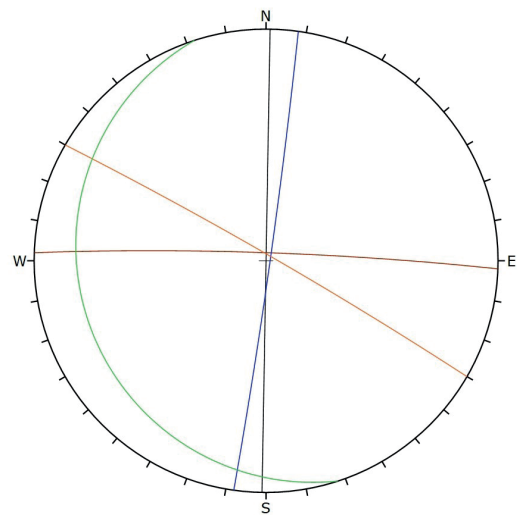


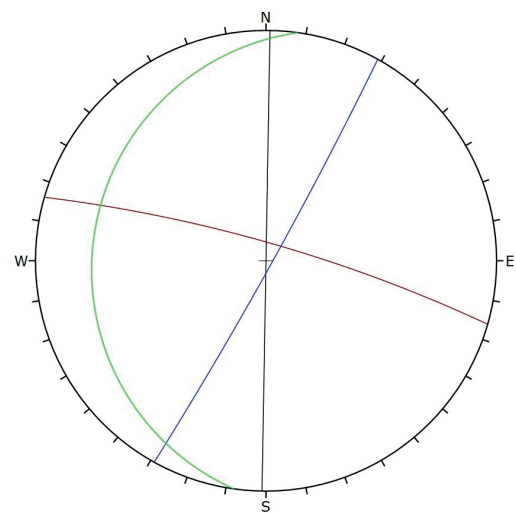
Fig. 1 Location and geology of the study area



(a)



(b)



(c)

Fig. 3 (a) Rock mass characterized by zone A and B, these areas have structural and lithological differences (b) Stereographic projection of zone A, (c) Stereographic projection of zone B

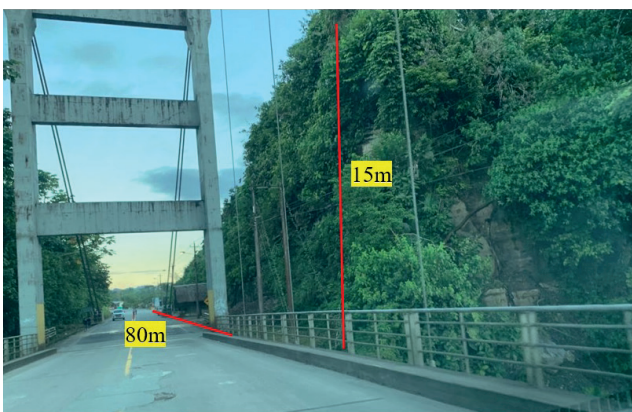


Fig. 2 Slope in contact with the bridge and road infrastructure. Some blocks can be seen at the foot of the slope

The study slope has a 90° slope, a total width of 80 m, and a height of 15 m at its highest point. The slope interacts with a section of the main highway, with the right abutment of the bridge over the Napo River and with cables and electric lighting poles (Fig. 2).

The rock mass is generally stratified. The upper part of the slope corresponds to a layer of soil-type material and is covered with vegetation. The rock mass underneath is characterized by two clearly differentiated zones. Zone A (Fig. 3), which has a sequence of shales, limestones, and calcareous sandstone, this zone has a thickness of 4m and three families of joints. Zone B (Fig. 3) corresponds to a less fractured limestone 4 m thick and presents two families of joints. The structural data of the two zones, we can see in Figs. 3(b), 3(c) and Table 1, respectively.

Table 1 Orientations of the plans

	Zone A Orientation (D/DD)	Zone B Orientation (D/DD)
J1	86/2	81/16
J2	88/98	87/119
J3	87/30	-
S0	12/252	16/278
SLO	90/91	

D dip, DD dip direction, SLO slope orientation, S0 bedding plane

2 Data and methods

2.1 Q-slope

We use the Q-slope method [12]. This method was developed by supplementing the Q index [13], originally developed to reinforce and support tunnels and caverns and designed for active use in rock outcrop characterization seismic velocity interpretations and borehole core logging [14]. Q-slope is a recent empirical method to assess the stability of rock slopes in the field. It is applied in different lithologies, civil engineering, and mining projects. It allows engineers to make adjustments to slope angles as excavation progresses without the need for reinforcement for slope heights of less than 30 m [15]. However, the Q-slope is applied to slope heights up to 250 m; typically recommended up to 50 m as per reference [16]. As in our case, the slope is 15 m, therefore it is in the range of application.

The calculation of the Q-slope requires six input parameters [12]:

$$Q_{-slope} = \frac{RQD}{J_n} * \left(\frac{J_r}{J_a} \right)_0 * \frac{J_{wice}}{SRF_{slope}}, \quad (1)$$

where:

$\frac{RQD}{J_n}$ is the crude measure of the relative block size, same as with the Q-index [14].

$\left(\frac{J_r}{J_a} \right)_0$ is the shear strength but has an orientation and "wedge" adjustment.

J_{wice} is the long-term exposure to various climatic and environmental conditions.

SRF_{slope} is the stress reduction factor for the slope, takes into account the physical conditions, stress, and orientation of the more significant discontinuities.

Barton and Bar [15] derived a simple equation for the steepest angle (β) In Eq. (2) and a chart depicted in Fig. 4, which allows prediction of the degree of slope stability. This chart (Fig. 4) is based on a database of almost 200 individuals [17]. Q-slope analyzes has been applied to igneous, sedimentary and metamorphic rocks, including saprolite-type materials in several countries [15].

$$\beta = 20 \log_{10} Q_{slope} + 65^\circ \quad (2)$$

In the abscissa axis of the stability chart (Fig. 4), the value of the Q-slope is entered, and on the ordinate axis, the slope angle in degrees. This chart allows knowing if the slope is stable, unstable, and uncertain conditions. The colored areas: green, red, and gray, show these three behaviors of the slope, respectively.

2.2 Seismic refraction tomography

We use a set of 24 geophones with a natural frequency of 4.5 Hz branched to a seismograph Geometrics-ES 3000. The processing software for picking the head-waves and the refraction tomography is the SeisImager/2D [18].

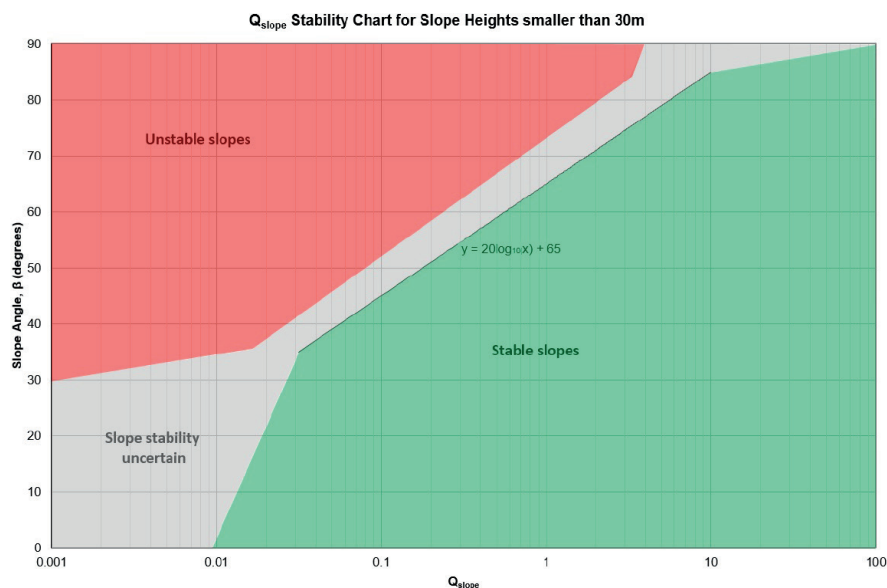


Fig. 4 Slope stability chart [15]

We installed a seismic line SL1 with azimuth 30° to the cliff using a road to avoid working on the tropical forest. The line is 115 m long with 24 geophones spaced 5 m (Fig. 5). We have produced 24 sledgehammer shots every 5 m and use these 24 records for the refraction tomography. We also use a second line SL2 with a 45 m length. SL2 is extended through the forest and is across the slope (Fig. 5).

The orientation of the joint geological sets is horizontal in the priori model of the tomography. The priori model is a flat layer model following the topography. The altitude of each geophone is introduced in the tomography software, and it designs the topography of the studying site [18]. The direct visual observation of the strata in the outcrop of the slope (Fig. 3) and the absence of significant evidence of folds in the studied regions [11] justify the choice of a horizontal flat layered model.

To obtain the priori model for the seismic tomography, we make preliminary inversions with the data. These inversions give a superficial velocity of 0.8 km/s and a 15 m depth velocity of 3.2 km/s. After, we find that 26 iterations of the code are enough to reach the convergence of the



Fig. 5 The red lines gives the positions of the two seismic lines: SL1 and SL2, used in this study. The dot-mark is the position of the borehole

solution. In Fig. 6 we show the convergence of the solution for different values of the horizontal smoothing parameter.

This parameter in the software has an inverse relation with the smoothing applied: 1.0 is not smoothing, and 0.3 is the solution with maximum smoothing.

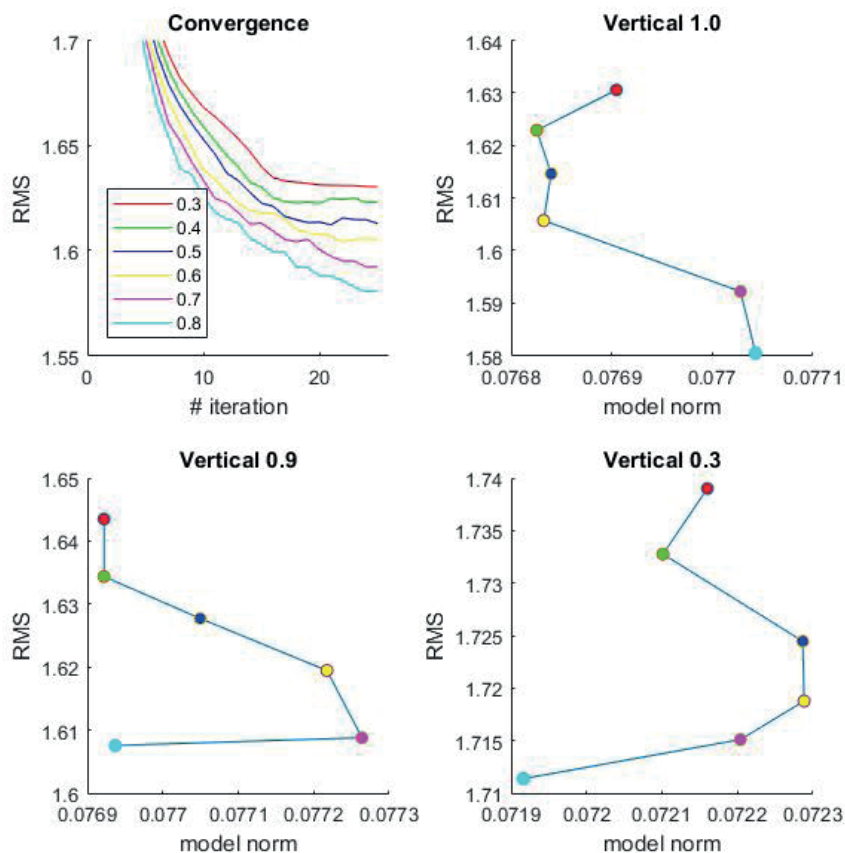


Fig. 6 Top left: the convergence of the solutions for different horizontal smoothing parameters given by colors. Top right: The L-curve for a vertical smoothing parameter of 1.0. The colors give the value of the horizontal parameter. Bottom left and right: L-curves for vertical smoothing of 0.9 and 0.3. The L-curve with vertical 1.0 gives the optimal solution in the corner horizontal 0.6

The problem of the refraction seismic tomography is the non-uniqueness of the solution [19]. To deal with this problem, we follow a regularization strategy based on the L-curve criterion [20]. We set a vertical smoothing value, and then we test all the solutions for all possible horizontal smoothing values from 0.3 to 0.8 in the SeisImager software. The solutions with horizontal smoothing 0.9 and 1.0 are oscillating and do not give a good convergence.

Then, we compute the norm of the model and plot these values versus the RMS obtained from the inversion. Fig. 2 gives the resulting L-curves for three vertical smoothing parameters: 1.0, 0.9, and 0.3. The colors define the value of the horizontal parameter.

From the three tests, the case with no vertical smoothing 1.0 gives the best concavity of the L-curve. From this L-curve, the corner is the horizontal parameter 0.6, which gives the optimal solution for our tomography problem.

The regularized solution for SL1 is in Fig. 7 (top panel).

We interpret the green color in Fig. 7 (top panel) as the Napo formation approximately 4.5 m below the surface. The seismic P wave velocity value obtained is 2.3 km/s. This tomographic model gives a representation of the continuity of the stratum.

The second tomographic model in Fig. 7 (bottom panel) for the SL2 gives us the velocity value for the Napo formation in the zone of the slope. This layer corresponds to a green color with 1.3 km/s for the seismic wave velocity. The P wave velocity is lower than the result in the line over

the road, due probably to the high weathering of the rocks below the rain forest. The 1.3 km/s is the value we can use in the following sections.

2.3 Seismic Q-slope using P-wave velocity

Barton [21] developed the $V-Q$ relationship, In Eq. (3). And order to include rock that could be weaker or oven stronger than the assumed "hard" rock, Q_c was introduce [16].

$$V_p = 3.5 + \log * Q \tag{3}$$

The Q -value and its modified form Q_c , obtained by normalizing with UCS/100, has many potentials uses in rock engineering. It can be correlated to the seismic P-wave velocity V_p (km/s) and Q -slope In Eqs. (4)–(6) [13, 22]. In Eq. (4), unconfined compressive strength (σ_c) in megapascals (MPa).

$$Q_c = \frac{\sigma_c}{100} * Q \tag{4}$$

$$Q_c = 10^{(V_p - 3.5)} \tag{5}$$

$$Q_{slope} = (Q_c)_0 * \frac{J_{wice}}{SRF_{slope}} \tag{6}$$

The Q_c value does not consider orientation factor (O-factor) and environmental and geological conditions number (J_{wice}), and the SRF_{slope} in most cases should be equal to one as stress reduction factors were already considered in the Q -value relationship with V_p [13].

In our case for Zone A, we take a value of $J_{wice} = 0.6$ according to Table 6 (wet environment - incompetent rock and stable structure) in [12].

2.4 Borehole

In the upper part of the slope, drilling with core recovery was carried out. The diameter of the recovered core was 10 cm. The drilling allowed us to relate the geophysical information, determine the thickness of the soil layer, and perform SPT test at 2.40 m depth (Fig. 8). The maximum depth of the borehole was 4.35 m (Fig. 9). The characterization of the soil layer that covers the massif A is important in this way, because [15] indicate the application of the Q -slope cannot be applied to soil masses, rock fill, or landslide debris.

The SPT was developed circa 1927, is performed by driving a standard split spoon sampler into the ground by blows from a drop hammer of mass 63.5 kg falling 760 mm. The sampler is driven 152 mm into the soil at the bottom of a borehole, and the number of blows (N) required to drive it

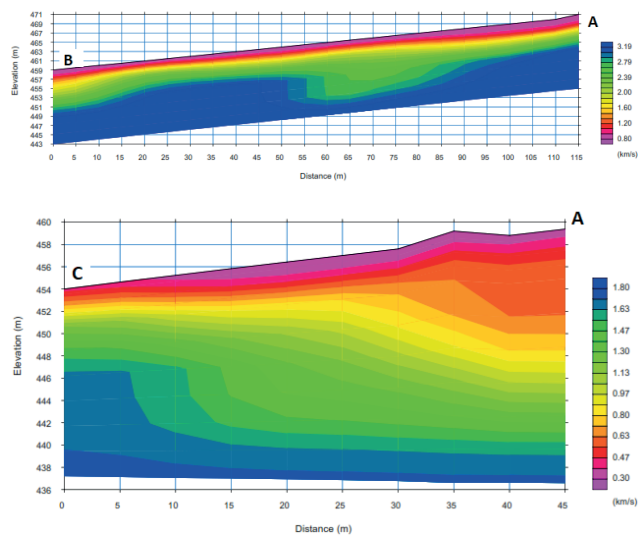


Fig. 7 The model obtained by seismic refraction tomography in the two seismic lines SL1 (top panel) and SL2 (bottom panel). The letters AB and AC give the sense of the cross-sections. Vertical and horizontal scales are in meters. P wave velocity is in km/s. The Napo formation is the green color with a seismic wave velocity of 2.3 km/s



Fig. 8 Borehole box shows three layers of soil. The first brown layer corresponds to a sandy clay soil (0.0 m to 0.75 m). The second dark brown layer corresponds to a plastic clay, with a low percentage of sand (0.75 m to 1.30 m). The third gray layer corresponds to a clayey sandy material (1.30 m to 4.35 m)



Fig. 9 The SPT test was performed on this material. This box shows the continuation of the third layer. This layer is where the SPT test was carried out

an additional 304 mm is counted. The number of blows (N) is called the standard penetration number. The advantage that lies in this is simple and quick to perform, and is very useful for determining changes in stratigraphy [23].

3 Results

SL2 and the borehole have defined a 7 m thick soil cover. The SPT test gave rejection at 2.50 m depth, indicating an increase in resistance in layer 3 (Fig. 8).

Two geomechanical stations were carried out in the lower part of the slope, these allowed collecting information of the intact rock and discontinuities, this information was used to calculate the Q-slope of the zone A (Q-slope A) and zone B (Q-slope B) directly applying Eq. (1).

One more Q-slope value of zone A (Q-slope A-SL2) was calculated from the SL2, in this case Eq. (6) was used introducing the value of V_p .

The values for the calculation of Q-slope A and Q-slope B are shown in Table 2, and the values of Q-slope A-SL2 in Table 3.

4 Discussion

Three Q-slope values were obtained, the resulting Q-slope A and Q-slope B values were calculated from data collected directly from the faces of each rock mass. The Q-slope A-SL2 value was calculated from the SL2. The seismic tomography line was also performed to determine the material coverage of the soil type. The decision to use geophysics was made because part of the massif in zone A is at a considerable height and covered with vegetation, making it difficult to access on foot.

Table 2 Q-slope value calculation factors

Q-slope		A	B
R_{QD}		90	95
J_n		15	6
J_r	SET A	1	2
	SET B	1	2
J_a	SET A	3	2
	SET B	3	2
0-factor	SET A	0.5	1
	SET B	0.8	1
J_{wice}		0.6	0.7
SRF_{slope}		10	2.5
Q_{-slope}		0.016	4.43

Table 3 Q-slope value calculation factors from SL2

V_p	1.3
Q_c	0.0063
J_{wice}	0.6
SRF_{slope}	1
$Q_{-slope} A-SL2$	0.00378

The values of Q-slope A and Q-slope A-SL2 are different, but, in general terms, both values show that the rock mass has a poor quality. This study observed that the Q-slope value of zone A, obtained from SL2, is lower than the one obtained from the front of the massif. The result of Q-slope B is higher than all, and this is because the rock mass has a competent structure, the orientation of the joints is quite favorable, and the SRF-slope value is low due to their physical conditions. Using the LS2 allows us to define the depth at which the rock massif is located and compare the Q-slope A-SL2 value with the Q-slope value obtained directly from the massif.

The criterion to divide the slope into two zones (A and B) was made based on the lithology and geological structure, assuming as if they were individual benches, in order to obtain a Q-slope value for each zone. This is possible according to [24] because the Q-slope can be used in road or rail cuttings or individual benches in open pit mines.

The SPT rejection value indicates that the hard soil begins at a depth of 2.50 m. This data is essential because it allows us to relate it to the SL2 information and determine how far this material advances, helping us to define the beginning of the massif.

Previous works compute quality rock mass coefficients using seismic tomography [1–7] in different scenarios and geological formations. However, there are no previous research works of Q determination in the organic-rich shales, limestones, and sandstones of the Napo formation, where the velocities in our study go from 1.8 km/s to 2.3 km/s.

Then, we can compare our results with limestones and shales of Bidu Formation [2], where the velocities vary between 2.5 km/s and 2.950 km/s and the Q_c varying from 0.04 to 5.012. In our case, the Q_c is 0.063, and the lower value is justified for the high weathering of the rock mass in the tropical zone.

The other previous work with similar results to our research is in the sandstones and shales of Malaysia's highways outcrops [4]. The velocities go from 0.75 km/s to 3.5 km/s, and the Q-System varies from 2.696 to 6.550. We cannot compare these results directly because we have

preferred computing the Q_c and the Q-slope. However, we can see low values in the seismic velocity due to weathering conditions of this tropical region similar to our study zone.

5 Conclusions

We have obtained two values of the wave velocity for the Napo Formation rocks: 2.3 km/s in the dried zone of the slope and 1.8 km/s in the weathered zone of the slope. These two values come from a seismic refraction tomography regularized using the method of the L-curve.

The values of Q-slope A (0.016) and Q-slope A-SL2 (0.00378) correlated very well and show that this area of the slope is of poor quality and unstable. The Q-slope B (4.43) indicates this zone presents uncertainty as to its stability, but due to its low height and the orientation of its structures, problems can be ruled out. Overall, the results show that the slope is unstable in zone A. A stable design can be achieved by setting the steepest slope angle and making a berm between the massifs.

Stability was assessed by focusing on the rocky part of the slope. However, for further study, it would be essential to complement the stability analysis by other methods that consider the geomechanical properties of the materials and the interaction of the soil layer above the massif.

Acknowledgements

Corrections made by two anonymous referees have been invaluable in this research.

References

- [1] Zhao, J. "Construction and utilization of rock caverns in Singapore Part A: The Bukit Timah granite bedrock resource", *Tunnelling and Underground Space Technology*, 11(1), pp. 65–72, 1996. [https://doi.org/10.1016/0886-7798\(96\)00054-5](https://doi.org/10.1016/0886-7798(96)00054-5)
- [2] Ghanbari, Y., Ramazi, H. R., Pazand, K., Madani, N. "Investigation of rock quality of Shirinrud dam site by engineering seismology", *Arabian Journal of Geosciences*, 6(1), pp. 177–185, 2013. <https://doi.org/10.1007/s12517-011-0322-7>
- [3] Carrozzo, M. T., Leucci, G., Margiotta, S., Mazzone, F., Negri, S. "Integrated geophysical and geological investigations applied to sedimentary rock mass characterization", *Annals of Geophysics*, 51(1), pp. 192–202, 2008. <https://doi.org/10.4401/ag-3044>
- [4] Mohd, S. N., Tan, A., Mohamad, E. T., Saad, R., bin Md Dan, M. F., Legiman, M. K. A. "Integration of geophysical interrogation and geomechanical assessment for sedimentary rock mass classification, Iskandar Puteri, Johor, Malaysia", *Malaysian Construction Research Journal*, 13(2), pp. 180–196, 2021. Available at: [online] <https://www.cream.my/my/publication/download-malaysian-construction-research-journal/mcrj-special-issues-volume-13-no-2-2021>
- [5] Butchibabu, B., Sandeep, N., Sivaram, Y. V., Jha, P. C., Khan, P. K. "Bridge pier foundation evaluation using cross-hole seismic tomographic imaging", *Journal of Applied Geophysics*, 144, pp. 104–114, 2017. <https://doi.org/10.1016/j.jappgeo.2017.07.008>
- [6] Heincke, B., Maurer, H., Green, A. G., Willenberg, H., Spillmann, T., Burlini, L. "Characterizing an unstable mountain slope using shallow 2D and 3D seismic tomography", *Geophysics*, 71(6), pp. 241–256, 2006. <https://doi.org/10.1190/1.2338823>
- [7] Yang, J., Dai, J., Yao, C., Jiang, S., Zhou, C., Jiang, Q. "Estimation of rock mass properties in excavation damage zones of rock slopes based on the Hoek-Brown criterion and acoustic testing", *International Journal of Rock Mechanics and Mining Sciences*, 126, Article number: 104192, 2020. <https://doi.org/10.1016/j.ijrmms.2019.104192>
- [8] Gelişli, K., Şeren, A., Babacan, A. E., Çataklı, A., Ersoy, H., Kandemir, R. "The Sumela Monastery slope in Maçka, Trabzon, Northeast Turkey: rock mass properties and stability assessment", *Bulletin of Engineering Geology and the Environment*, 70(4), pp. 577–583, 2011. <https://doi.org/10.1007/s10064-010-0343-6>

- [9] Baby, P., Rivadeneira, M., Barragán, R. "La Cuenca Oriente: Geología y Petróleo" (The Eastern Basin: geology and oil), Institut français d'études andine, Lima, Peru, 2004. (in Spanish)
<https://doi.org/10.4000/books.ifea.2971>
- [10] Baldock, J. "Geología del Ecuador" (Geology of Ecuador), Ministerio de Recursos Naturales y Energéticos, Dirección General de Geología y Minas, Quito, Ecuador, 1982. (in Spanish)
- [11] Egüez, D. A., Gaona, M., Albán, A. "Mapa Geológico de la República del Ecuador" (Geological Map of the Republic of Ecuador), Instituto de Investigación Geológico y Energético, Quito, Ecuador, [map] Available at: https://www.geoenergia.gob.ec/wp-content/uploads/downloads/2021/06/Mapa-Ggeologico_ecuador-2017_compressed.pdf [Accessed: 15 June 2021] (in Spanish)
- [12] Bar, N., Barton, N. "The Q-slope Method for Rock Slope Engineering", *Rock Mechanics and Rock Engineering*, 50(12), pp. 3307–3322, 2017.
<https://doi.org/10.1007/s00603-017-1305-0>
- [13] Bar, N., Barton, N. "Rock Slope Design using Q-slope and Geophysical Survey Data", *Periodica Polytechnica Civil Engineering*, 62(4), pp. 893–900, 2018.
<https://doi.org/10.3311/PPci.12287>
- [14] Barton, N., Lien, R., Lunde, J. "Engineering classification of rock masses for the design of tunnel support", *Rock Mechanics*, 6(4), pp. 189–236, 1974.
<https://doi.org/10.1007/BF01239496>
- [15] Barton, N., Bar, N. "Introducing the Q-slope method and its intended use within civil and mining engineering projects", In: *Proceedings of ISRM Regional Symposium Eurock 2015 & 64th Geomechanics Colloquium Eurock 2015*, Salzburg, Austria, 2015, pp. 157–162.
- [16] Barton, N. "Some new Q-value correlations to assist in site characterisation and tunnel design", *International Journal of Rock Mechanics and Mining Sciences*, 39(2), pp. 185–216, 2002.
[https://doi.org/10.1016/S1365-1609\(02\)00011-4](https://doi.org/10.1016/S1365-1609(02)00011-4)
- [17] Bar, N., Barton, N. "Empirical slope design for hard and soft rocks using Q-slope", In: *Proceedings of the 50th US Rock Mechanics / Geomechanics Symposium ARMA 2016*, Houston, TX, USA, 2016, ARMA16-384.
- [18] Geometrics Inc. "SeisImager/2DTM Manual (Version 3.3)" [pdf] 2009. Available at: https://geometrics.com/wp-content/uploads/2019/05/SeisImager2D_Manual_v3.3.pdf
- [19] Hayashi, K. "Non-Uniqueness in Seismic Refraction Analysis", In: *24rd EEGS Symposium on the Application of Geophysics to Engineering and Environmental Problems*, Charleston, SC, USA, 2011, pp. 40–52.
<https://doi.org/10.4133/1.3614108>
- [20] Hansen, P. C. "Analysis of discrete ill-posed problems by mean of the L-curve", *Society for Industrial and Applied Mathematics*, 34(4), pp. 561–580, 1992.
<https://doi.org/10.1137/1034115>
- [21] Barton, N. "Rock Quality, Seismic Velocity, Attenuation and Anisotropy", Taylor & Francis, London, UK, 2006.
<https://doi.org/10.1201/9780203964453>
- [22] Barton, N., Grimstad, E. "Q-system - An illustrated guide after 40 years in Tunnelling", [online] Available at: http://www.nickbarton.com/downloads_04.asp [Accessed: 2 June 2021]
- [23] Budhu, M. "Soil Mechanics and Foundations", Wiley, New York, NY, USA, 2000.
- [24] Bar, N., Barton, N. "The Q-Slope: An Empirical Rock Slope Engineering Approach in Australia", *Australian Geomechanics Journal*, 53(4), pp. 73–86, 2018.